EFDA–JET–PR(08)26

K. Crombé, Y. Andrew, T.M. Biewer, E. Blanco, P.C. de Vries, C. Giroud,
N.C. Hawkes, A. Meigs, T. Tala, M. von Hellermann, K.-D. Zastrow
and JET EFDA contributors

Radial Electric Field in JET Advanced Tokamak Scenarios with Toroidal Field Ripple

Radial Electric Field in JET Advanced Tokamak Scenarios with Toroidal Field Ripple

K. Crombé[1], Y. Andrew[2], T.M. Biewer[3], E. Blanco[4], P.C. de Vries[2], C. Giroud[2], N.C. Hawkes[2], A. Meigs[2], T. Tala[5], M. von Hellermann[6], K.-D. Zastrow[2] and JET EFDA contributors*

JET-EFDA, Culham Science Centre, OX14 3DB, Abingdon, UK

[1]Postdoctoral Fellow of the Research Foundation - Flanders (FWO), Department of Applied Physics, Ghent University, Rozier 44, B-9000 Gent, Belgium
[2]EURATOM-UKAEA Fusion Association, Culham Science Centre, OX14 3DB, Abingdon, OXON, UK
[3]Oak Ridge National Laboratory, Oak Ridge, TN 37831-6169, Tennessee, USA
[4]Laboratorio Nacional de Fusion, Asociacion EURATOM-CIEMAT, Madrid, Spain
[5]VTT Technical Research Centre of Finland, Association EURATOM-Tekes, P.O. Box 1000, FIN-02044 VTT, Finland
[6]FOM Institute for Plasma Physics Rijnhuizen, Association EURATOM-FOM, Trilateral Euregio Cluster, PO Box 1207, 3430 BE Nieuwegein, The Netherlands
** See annex of F. Romanelli et al, "Overview of JET Results ", (Proc. 22nd IAEA Fusion Energy Conference, Geneva, Switzerland (2008)).*

Preprint of Paper to be submitted for publication in
Plasma Physics and Controlled Fusion

ABSTRACT.
A dedicated campaign has been run on JET to study the effect of Toroidal Field (TF) ripple on plasma performance. Radial electric field measurements from experiments on a series of plasmas with internal transport barriers and different levels of ripple amplitude are presented. They have been calculated from charge exchange measurements of impurity ion temperature, density and rotation velocity profiles, using the force balance equation. The ion temperature and toroidal and poloidal rotation velocities are compared in plasmas with both reversed and optimised magnetic shear profile. Poloidal rotation velocity (v_θ) in the ITB region is measured to be of the order of a few tens of km/s, significantly larger than the neoclassical predictions. Increasing levels of TF ripple are found to decrease the ITB strength and maximum value of v_θ. The poloidal rotation term dominates in the calculations of the total radial electric field (E_r) and **E×B** shearing rate, with the largest gradient in E_r measured in the radial region coinciding with the ITB.

1. INTRODUCTION

Toroidal Field (TF) ripple has been shown to affect the toroidal rotation velocity (v_θ) profiles in tokamaks through enhanced losses of fast and thermal ions [1, 2]. The ripple amplitude is defined as the relative variation of the magnetic field at the separatrix, $\delta = (B_{max} - B_{min})/(B_{max} + B_{min})$. For standard JET plasmas $\delta = 0.08\%$, while for ITER it will be of the order of $\delta = 0.5\%$. By independently powering the odd and even-numbered toroidal field coils the JET ripple was increased up to $\delta = 1.00\%$.

On JET dedicated experiments in the Advanced Tokamak (AT) regime were performed to study the formation and sustainment of Internal Transport Barriers (ITBs) in the presence of TF ripple. It has been found that ITBs are triggered even in plasmas with ripple amplitude $\delta = 1.00\%$, but the ITB strength is reduced for high as compared to standard operation [3].

It was found in previous experiments that the poloidal rotation velocity in the ITB region is significantly higher than neoclassical values for JET plasmas with standard ripple amplitude [4]. In this paper measured poloidal rotation velocity profiles are presented in ITB plasmas with gradually increasing δ. They are then used to calculate fully experimental profiles of the radial electric field and **E×B** shearing rates. Rotational shear has been linked to turbulence suppression and is believed to play a crucial role in the dynamics of edge and core transport barriers [5, 6, 7, 8]. The experimental v_θ measurements are compared to neoclassical calculations from the NCLASS module embedded in the JETTO transport code. ITBs in discharges with strongly reversed q-profiles are compared to plasmas with monotonic or weakly reversed q.

2. EXPERIMENTAL RESULTS

Two sets of four shots are presented for which the ripple amplitude was gradually increased: $\delta = 0.08\%$, $\delta = 0.63\%$, $\delta = 0.82\%$ and $\delta = 1.00\%$. In one set Lower Hybrid Current Drive (LHCD) was used during the current ramp-up to create a radial zone with strongly negative magnetic shear, the

so-called Reversed Shear (RS) scenario, while the second set did not have LHCD and the q-profile is monotonic or weakly reversed, the so-called Optimised Shear (OS) scenario. The RS plasmas were run with B_t/I_p = 2.2T/1.8MA and the OS plasmas with B_t/I_p = 2.2T/1.9MA. The Neutral Beam heating (NBI) varied between 10.0MWand 13.2MW, and between 3.0MWand 3.8MW of off-axis Ion Cyclotron Resonant Frequency heating (ICRH) was applied at 37MHz. The ion temperature (T_i) and toroidal (v_ϕ) and poloidal (v_θ) rotation velocities are measured by Charge eXchange Recombination Spectroscopy (CXRS) on fully ionised carbon impurities at a wavelength λ = 529.1 nm. The electron temperature (T_e) is measured by electron cyclotron emission and electron densities (n_e) are measured by the Thomson scattering diagnostic. q-profile measurements are obtained using the Motional Stark Effect measurements.

In figure 1 (a) time traces of T_i and T_e are plotted at R = 3.2m, corresponding to normalised radius λ = r/a = 0.13, as well as the electron density (b), the diamagnetic and thermal energy (c), and the additional heating power (d) for one of the shots with reversed and one with optimised magnetic shear. In both pulses the ripple amplitude was δ = 0.63%.

2.1. GENERAL PARAMETERS

In figures 2 (a) and (b) the ion and electron temperature profiles are shown for the same pulses as in figure 1. The profiles in red are for a time before the start of the ITB phase and the ones in blue for a time around the maximum in ITB strength that was reached during the pulse, defined by the T_i criterion [9]. Figures 2 (c) and (d) show the angular frequency profiles, (e) and (f) are the electron density and (g) and (h) illustrate the difference in q-profile between the RS and OS case.

From the temperature profiles it can be seen that the foot of the ITB is around ρ = 0.65 in both cases for the ions and slightly more inwards for the electrons. The T_i gradient is sharper for the RS barrier and the central value slightly higher, 12.5keV compared to 11.5keV for the OS barrier. The ITB can also be observed from the angular frequency profiles, central values reach 100–120 krad/s at R = 3.10m, while for $\rho > 0.90$ (corresponding to R = 3.79m) the plasma counter rotates relative to the plasma current up to a maximum value of –20krad/s at R = 3.84m due to the enhanced ripple.

For the poloidal rotation the positive direction is in the electron diamagnetic drift velocity direction, i.e. for JET upwards at the outer half of the plasma radius.

2.2. ION TEMPERATURE AND ROTATION VELOCITIES

Four discharges have been selected with RS profile. The ripple amplitude of the different shots is given in table 1 as well as the maximum ρ^*_{Ti}. The profiles on the left hand side of figure 3 (a,c,e) are for a time t_1 between 50 and 500 ms before the start of the ITB (the time t1 is given in table 1). The start time of the ITB is taken when T_i exceeds the empirical value for JET of 0.014, as it was found in [9]. The profiles on the right hand side (b,d,f) are for a time t2 around the maximum of the ITB given in table 1. Figure 3 shows T_i ((a) and (b)), toroidal rotation velocity v_θ ((c) and (d)) and poloidal rotation velocity v_θ ((e) and (f)), combining the data from the core and edge CXRS

diagnostics [10, 11]. The highest central T_i is 15keV and is reached for Pulse No: 69670, with the standard JET ripple $\delta = 0.08\%$. This plasma also had the largest toroidal and poloidal rotation velocities. In figures 3 (c) and (d) it can be seen that the toroidal rotation velocity is strongly affected by increasing δ [2]; in the pre-ITB phase an edge zone of about 7cm width in counter rotation is observed for ripple amplitude $\delta = 0.63\%$ (Pulse No: 69665), extending from the scrape-off-layer inwards up to $\delta = 0.87$. For $\delta = 1.00\%$ (Pulse No: 69690) this zone extends up to $\delta = 0.70$ and is about 20cm wide.

The barrier strength decreases with increasing ripple. In figure 3 (e) it can be seen that v_θ at around $\delta = 0.35$ is between 3 and -35 km/s at t_1, i.e. prior to when the ITB criterion is exceeded. This value is obtained early on during the main heating phase and remains at the same level for several seconds. No sign of a transient spin-up just before the start of the ITB is measured with the present time resolution of the diagnostic at 50ms. Although $T_i > 0.014$ is only reached for t = 5.25s, signs of a weak barrier ($\rho^*_{Ti} > 0.010$) are present in Pulse No: 69670 from t = 3.85s on, coinciding with the measured increase of v_θ from -3 ($+-5$ km/s) to -35 km/s ($+-12$ km/s) at the innermost viewing chord. An increase to a maximum of -60 km/s is observed in figure 3 (f), well into the ITB phase. The poloidal rotation profile for $0.55 < \rho < 0.80$ (corresponding to a radial width of 17cm) is almost flat and <20km/s at t_1, but spins up to between 35 and 75km/s in positive direction at t_2, with the peak value at the foot of the ITB.

For Pulse No: 69670 the radial correlation reflectometer was taking data during the time interval t = [5.50s, 5.82s], around the maximum strength of the ITB. Figure 4(a) shows the phase of the reflected signal at R = 3.48m (corresponding to $\rho = 0.46$), using the 76 GHz fixed frequency channel. At t = 7.30s the slope of the average signal changes sign, which possibly indicates a reversal of the direction of the poloidal rotation velocity of the density fluctuations. This time coincides with the decrease (in absolute values) of the impurity ion poloidal rotation velocity, as seen in different channels of the CXRS diagnostic ($\rho = 0.35$ to $\rho = 0.68$), after reaching peak values at about t = 7.25s (figure 4(b)). However, due to the limited time resolution of the electron density measurements in this time interval, it is not possible to exclude movements of the cutoff layer which could account for some of the observed variations in phase drift. Also, the reflectometer on JET is not a Doppler reflectometer, therefore no absolute values of the rotation velocity of the fluctuations could be derived.

In figure 5 the equivalent profiles to those in figure 3 are depicted, for a series of four OS discharges, specified in table 2. Generally the OS ITBs are weaker than the RS series and the central T_i is 11 keV for all shots. Similarly to the RS series the ITB strength decreases with increasing, and the edge toroidal rotation profile shows a counter ro-tating zone that extends further inwards with increased ripple. The poloidal rotation profiles at t1 (e) are relatively similar to the profiles for the RS shots before the ITB phase. No spin-up in the negative direction is observed around = 0.30 at t_2. At the foot of the barrier the maximum v is 40 km/s for Pulse No: 69676 with = 0.08% and 15 km/s for 69679 with $\delta = 1.00\%$.

2.3. EXPERIMENTAL POLOIDAL ROTATION IN RADIAL ELECTRIC FIELD CALCULATIONS

The measured v_θ profile of the carbon impurity ions for Pulse No: 69665 and 69677 is plotted in figures 6 (a) and (b) respectively, as well as the neoclassical predictions by NCLASS [12]. The JETTO simulations are done interpretatively, using the profiles from figures 3 and 5 for ion temperature and toroidal rotation velocity, with combined core and edge CXRS measurements, as input. The poloidal rotation measurements are limited to the radial region $\rho > 0.3$. For $\rho < 0.3$ the poloidal rotation velocities were set to zero and therefore the simulated profiles are only meaningful for $\rho > 0.3$. JETTO creates a smooth transition between the last point of the experimental profile and the zero level for $\rho < 0.3$. It can be seen that the experimental values for v_θ are very different from the neoclassical predictions for main and impurity ions in the ITB region, further confirming previous results on JET [4]. For the RS case a maximum velocity of 45km/s is reached in the electron diamagnetic drift direction and −27km/s in the ion diamagnetic drift direction. The OS barrier was weaker and v_θ only reaches around 20−25km/s in both directions.

The radial electric field E_r profiles are plotted in figures 6 (c) and (d). They have been calculated using the force balance equation for carbon impurity ions:

$$E_r = \frac{1}{Zen_z}\frac{dp_z}{dr} - (v_\theta B_\phi - v_\phi B_\theta), \tag{1}$$

where Z is the impurity ion charge number, e is the electron charge, p_Z is the impurity pressure and n_Z the impurity density, B_θ is the poloidal magnetic field and B_ϕ the toroidal magnetic field. Carbon density, temperature and rotation velocities have been measured using charge exchange recombination spectroscopy. Due to the relatively large importance of the term $-v_\theta B_\phi$ term, the Er profiles are strongly affected by the high poloidal rotation velocities in the ITB region. In figures 6 (c) and (d) it can be seen that the global shape of the experimental E_r profile is in fact dominated by the shape of the v_θ profile. A strong gradient in E_r is observed in the region $\rho = 0.3-0.5$ when using the experimental values instead of the NCLASS predictions, again confirming results in [4].

3. COMPONENTS RADIAL ELECTRIC FIELD AND EXB SHEARING RATES

Three terms in equation (1) contribute to the total electric field and the Hahm-Burrell shearing rate ($\omega_{E\times B}$) given by [13]:

$$\omega_{E\times B} = \left| \frac{RB_\theta}{B_\phi}\frac{\delta}{\delta\psi}\left(\frac{E_r}{RB_\theta}\right)\right| \tag{2}$$

The individual terms in the radial electric field and the total Er are plotted in figure 7 for both the RS and OS series. The pressure gradient is the weakest contribution, even for the strongest barrier without ripple (Pulse No's: 69670). The toroidal rotation term is largest for the no-ripple case and decreasing with increasing δ consistent with the known effect of ripple on toroidal rotation [1, 2].

The largest contribution to the total E_r is caused by the strong poloidal rotation in the region with strong T_i gradient $0.20 < \rho < 0.75$. The largest poloidal rotation is observed for the strongest ITBs (Pulse No's: 69670, 69665 and 69676, 69677). For the weaker barriers (Pulse No's: 69684, 69690 and 69682, 69679) the contribution from the poloidal rotation also dominates the shape of the total E_r. These observations indicate that the amplitude of the poloidal rotation velocity is linked to the strength of the ITB and plays a significant role in the rotational shear and its link to turbulence suppression. The maximum poloidal rotation decreases with increasing TF ripple amplitude, but cannot be separated from the accompanied decrease in ITB strength. From the present dataset it is not clear whether the ripple affects the poloidal rotation or ρ^*_{Ti} . In all shots the radial region with strongest ρ^*_{Ti} gradient coincides with the strongest Er gradient.

The total shearing rate and its separate contributions are plotted in figure 8. As in the E_r profiles, the weakest contribution is from the pressure gradient. For the RS series the toroidal rotation contribution decreases with increasing ripple, but no clear dependence is seen in the OS case. The large poloidal rotation term also dominates the shape of the shearing rate, again both for the RS and OS series. The radial zone with the strong T_i gradient associated with the ITB ($0.25 < \rho < 0.55$) shows an increased $\omega_{E\times B}$. The total shearing rate for the shots with stronger ripple ($\delta = 0.82\%$ and $\delta = 1.00\%$) does not seem to depend on the q-profile, while for $\delta = 0.08\%$ and $\delta = 0.63\%$ the shearing rate is 50 % weaker in the OS as compared to RS discharges.

SUMMARY

ITB plasmas with different levels of TF ripple have been compared, ranging from the standard $\delta = 0.08\%$ for JET operations up to a maximum $\delta = 1.00\%$. The first series has a strongly reversed q-profile, while the second series had a monotonic or weakly reversed q. ITBs are triggered in both reversed and optimised shear plasma, but grow stronger in the RS case, when also the total Er and $\omega_{E\times B}$ are also at their strongest. Large TF ripple leads to weaker barriers. Toroidal rotation profiles are directly affected by the ripple, for $\delta = 1.00\%$ the radial edge zone of counter rotation extends inwards up to $\rho = 0.70$, which corresponds to a radial layer of about 20cm. No clear dependence of the ripple on the poloidal rotation prior to the ITB formation is seen. During the ITB phase a stronger barrier is associated with the occurance of an increased poloidal rotation. Increasing δ leads to lower values of v_θ, but also decreases the maximum ρ^*_{Ti}, and therefore the effects cannot be separated. The measured poloidal rotation is up to 20 times larger than the neoclassical predictions and contributes more than 50% to the total radial electric field profile and shearing rate, which is believed to break up turbulent eddies and reduce transport.

ACKNOWLEDGMENTS

This work, supported by the European Communities and the Royal Military Academy (RMA), Belgium, has been carried out within the framework of the European Fusion Development Agreement under the Contract of Association between EURATOM and the Belgian State. Financial support

was also received from Ghent University (UG), Belgium, and the Research Foundation - Flanders (FWO). The views and opinions expressed herein do not necessarily reflect those of the European Commission, RMA, UG or FWO.

REFERENCES

[1]. Urano H. et al., Nucl. Fusion (2007), Vol. **47**, 706-713
[2]. de Vries P.C. et al., Nucl. Fusion (2008), Vol. **48**, 035007
[3]. de Vries P.C. et al., Plasma Phys. Control. Fusion (2008), Vol. **50**, 065008
[4]. Crombé K. et al., Phys. Rev. Lett. (2005), Vol. **95**, 155003
[5]. Burrell K.H., Plasma Phys. Control. Fusion (2006), Vol. **48**, A347-A363
[6]. Connor J. et al., Nucl. Fusion (2004), Vol. **44**, R1
[7]. Hidalgo C. , Plasma Phys. Control. Fusion (1995), Vol. **37**, A53-A67
[8]. Gohil P. et al., Plasma Phys. Control. Fusion (1995), Vol. **37**, A53-A6
[9]. Tresset G. et al., Nucl. Fusion (2002), Vol. **42**, 520
[10]. Negus C. et al., Rev. Sci. Instrum. (2006), Vol. **77**, 10F102
[11]. Andrew Y. et al., Rev. Sci. Instrum. (2006), Vol. **77**, 10E913
[12]. Houlberg W. et al., Phys. Plasmas (1997), Vol. **4**, 3230
[13]. Hahm T.S. and Burrell K.H., Phys. Plasmas (1995), Vol. **2**, 1648

Pulse No:	δ (%)	I_{min}/I_{max}	max ρ^*_{Ti}	t_1 (s)	t_2 (s)
69670	0.08	1.00	0.040	4.725	5.725
69665	0.63	0.66	0.039	5.525	6.025
69684	0.82	0.59	0.026	4.375	6.275
69690	1.00	0.50	0.024	4.125	5.675

Table 1: Shots with RS

Pulse No:	δ (%)	I_{min}/I_{max}	max ρ^*_{Ti}	t_1 (s)	t_2 (s)
69676	0.08	1.00	0.028	4.375	5.125
69677	0.63	0.66	0.029	4.375	5.225
69682	0.82	0.59	0.024	4.475	4.485
69679	1.00	0.50	0.023	4.325	4.875

Table 2. Shots with OS

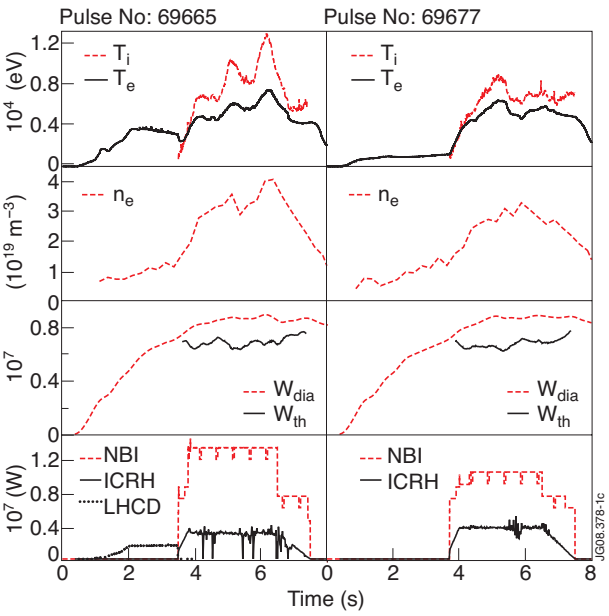

Figure 1: Time traces of (a) ion and electron temperature at R=3.2m ($\rho \approx 0.13$), (b) electron density at R=3.2m, (c) diamagnetic and thermal energy (W_{dia} and W_{th}) and (d) additional heating power for Pulse No's: 69665 with RS and 69677 for OS with = 0.63%.

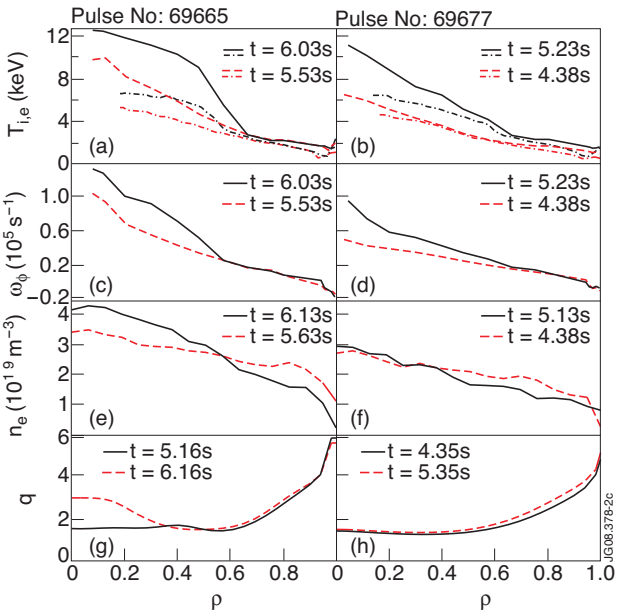

Figure 2: Profiles of (a-b) ion and electron temperature, (c-d) angular frequency, (e-f) electron density and (g-h) q-profile for Pulde No's: 69665 (a,c,e,g) with RS and 69677 (b,d,f,h) with OS. Both shots have ripple amplitude $\delta = 0.63\%$ and profiles are shown before (red) and during (blue) the ITB phase, for the times indicated in tables 1 and 2.

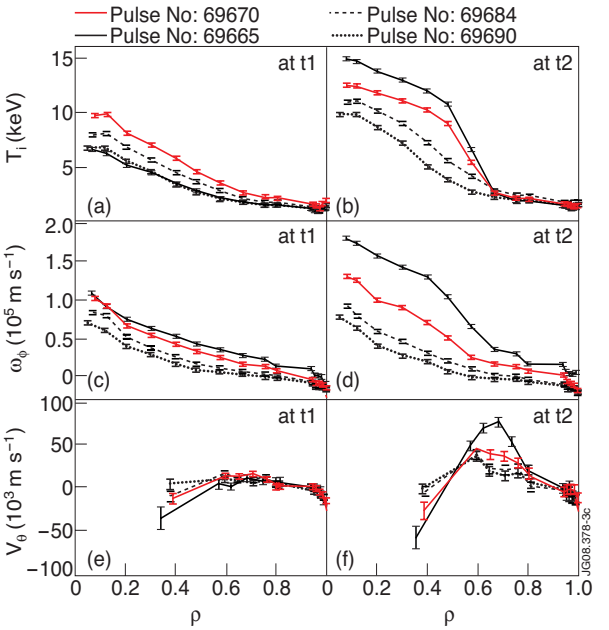

Figure 3: (a-b) ion temperature, (c-d) angular frequency and (e-f) poloidal rotation velocity for the series of four RS shots with different ripple amplitude, before the start of the ITB on the left hand side, and around the maximum of the ITB strength on the right hand side for the times indicated in table 1.

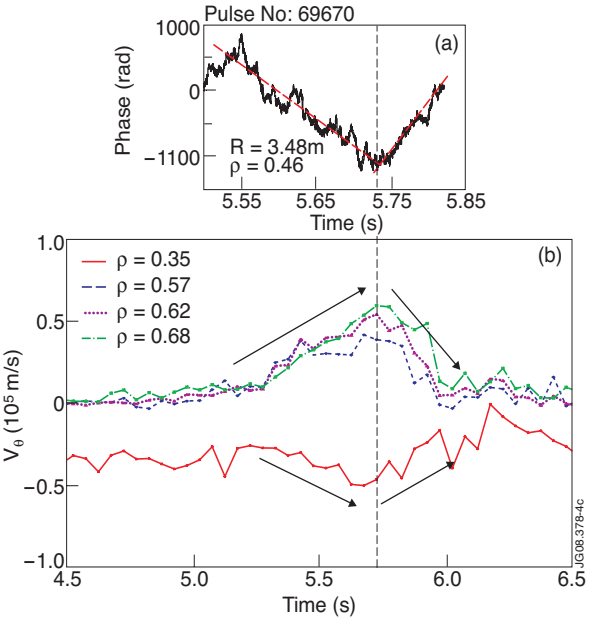

Figure 4: (a) Time evolution of the phase of the reflected signal at ρ = 0.46, measured by the reflectometer diagnostic. (b) Time evolution of the poloidal rotation velocity of the carbon C^{6+} impurity ions at the different radial locations.

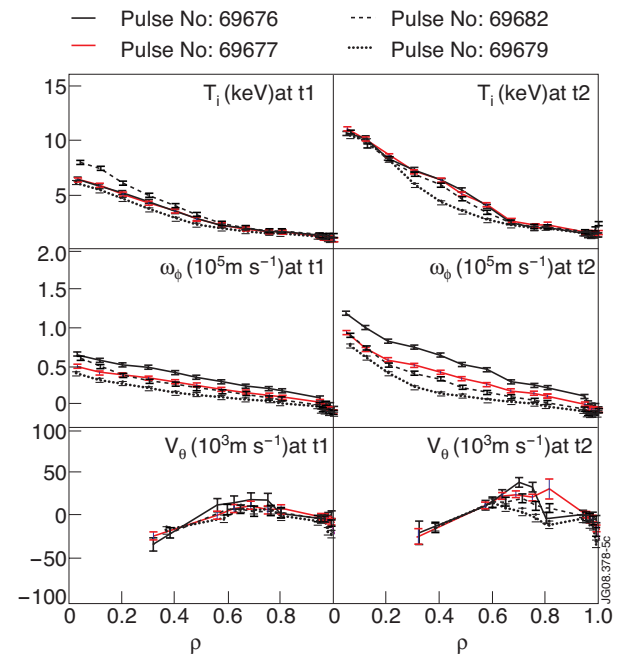

Figure 5: (a-b) ion temperature, (c-d) angular frequency and (e-f) poloidal rotation velocity for the series of four OS shots with different ripple amplitude, before the start of the ITB on the left hand side, and around the maximum of the ITB strength on the right hand side for the times indicated in table 2.

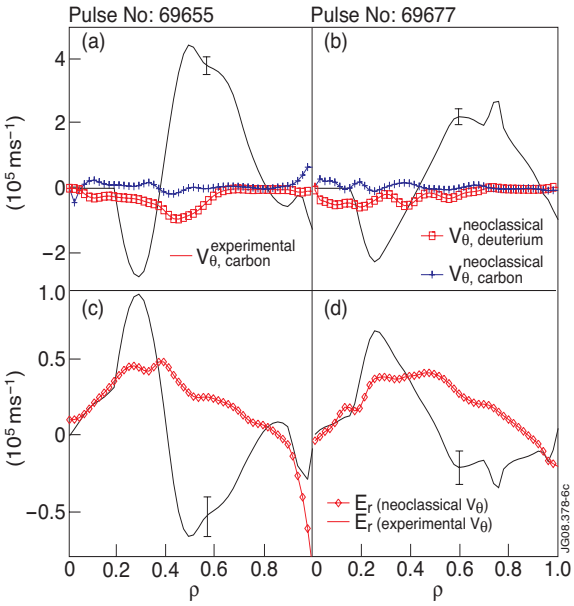

Figure 6: (a) and (b) experimental poloidal rotation velocity and neoclassical predictions by NCLASS for main ions and carbon impurities for Pulse No's: 69665 and 69677. (c) and (d) Radial electric field profiles using the experimental and neoclassical poloidal rotation.

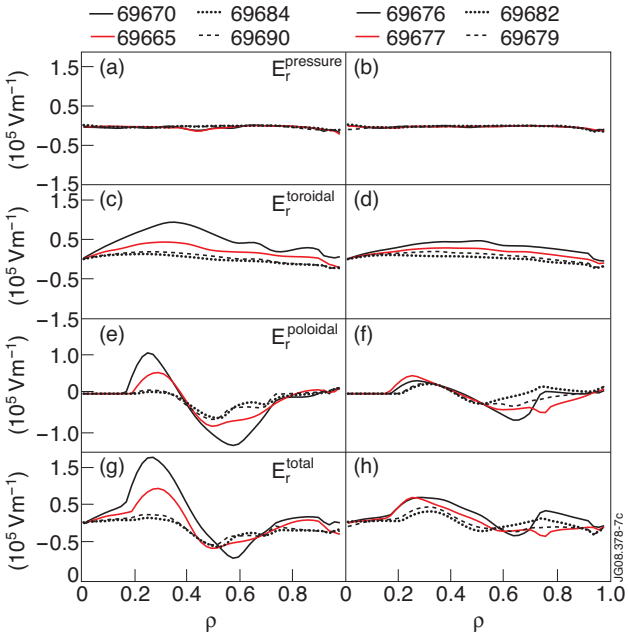

Figure 7: Different components of the radial electric field for the RS series on the left hand side and for the OS series on the right hand side at the ITB maximum strength. (a-b) Pressure gradient term $1/Zen_Z\, dp_Z/dr$, (c-d) toroidal rotation velocity term $v_\phi B_\theta$, (e-f) poloidal rotation velocity term $-v_\phi B_\theta$, (g-h) total E_r.

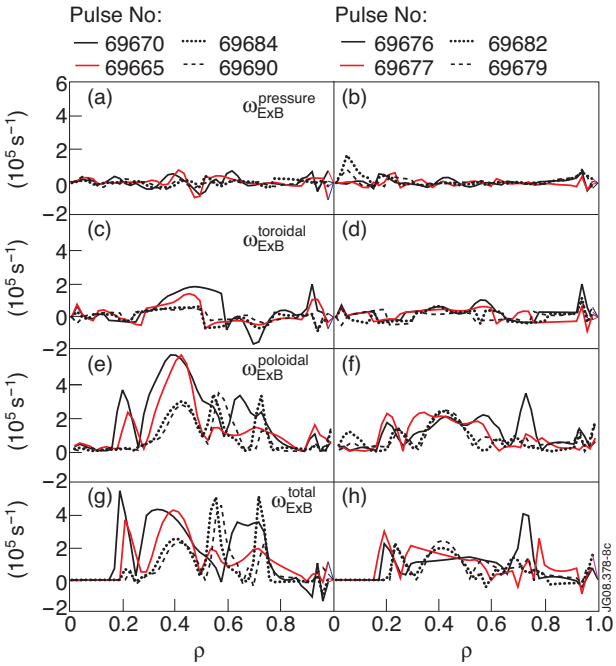

Figure 8: Different parts of the $\omega_{E\times B}$ shearing rate corresponding to the equivalent components of E_r, (a-b) pressure gradient, (c-d) toroidal rotation velocity, (e-f) poloidal rotation velocity, (g-h) total $\omega_{E\times B}$.